Astron. Astrophys. 346, 785–797 (1999)

ASTRONOMY AND ASTROPHYSICS

Mapping the contours of the Local bubble: preliminary results⋆

D.M. Sfeir[1,2], R. Lallement[1], F. Crifo[3], and B.Y. Welsh[2]

[1] Service Aéronomie du CNRS, F-91371 Verrières-le-Buisson, France
[2] Experimental Astrophysics Group, Space Sciences Laboratory, Berkeley, USA
[3] DASGAL and URA 335 du CNRS, Observatoire de Paris, F-92195 Meudon, France

Received 22 February 1999 / Accepted 26 March 1999

Abstract. We present preliminary results from a long-term program of mapping the neutral absorption characteristics of the local interstellar medium, taking advantage of Hipparcos stellar distances. Equivalent widths of the NaI D-line doublet at 5890 Å are presented for the lines-of-sight towards some 143 new target stars lying within 300 pc of the Sun. Using these data which were obtained at the Observatoire de Haute Provence, together with previously published NaI absorption measurements towards a further 313 nearby targets, we present absorption maps of the distribution of neutral gas in the local interstellar medium as viewed from 3 different galactic projections. In particular, these maps reveal the Local Bubble region as a low neutral density interstellar cavity in the galactic plane with radii between 65–250 pc that is surrounded by a (dense) neutral gas boundary (or "wall"). We have compared our iso-column contours with the contours derived by Snowden et al. (1998) using ROSAT soft X-ray emission data. Consistency in the global dimensions derived for both sets of contours is found for the case of a million degree hot LB plasma of emissivity $0.0023\,\mathrm{cm}^{-6}\,\mathrm{pc}$ with an electron density of $0.005\,\mathrm{cm}^{-2}$. We have detected only one relatively dense accumulation of cold, neutral gas within 60 pc of the Sun that surrounds the star δ Cyg, and note that the nearest molecular cloud complex of MBM 12 probably resides at the very edge of the Local Bubble at a distance of ~ 90 pc. Our observations may also explain the very different physical properties of the columns of interstellar gas in the line-of-sight to the two hot stars ϵ CMa and β CMa as being due to their locations with respect to the Bubble contours. Finally, in the meridian plane the LB cavity is found to be elongated perpendicularly to the Gould's Belt plane, possibly being "squeezed" by the expanding shells of the Sco-Cen and Perseus-Taurus OB associations.

Key words: ISM: bubbles – ISM: structure – Galaxy: solar neighbourhood

⋆ Tables 1 and 2 are also available in electronic form at the CDS (Strasbourg) via anonymous ftp to cdsarc.u-strasbg.fr (130.79.128.5) or via http://cdsweb.u-strasbg.fr/Abstract.html

1. Introduction

The characteristics of the plasma that fills the so-called 'Local Bubble' (hereafter LB), a large volume of rarefied gas that surrounds the Sun, are still a matter of much debate. It is believed that the LB, the possible result of a past supernova event, is mainly filled with hot gas with a temperature of more than one million K, and is the source of the ubiquitous soft X-ray diffuse background emission (Snowden et al. 1998). Although information on the very diffuse gas clouds embedded in the LB can easily be obtained through use of high resolution absorption spectroscopy towards nearby stars (Lallement et al. 1995; Crawford et al. 1997) obtaining information on the distribution and physical properties of the hot gas is not as straightforward. For example, it is still uncertain whether the highly ionized species (i.e. CIV, SiIV and OVI) and the 10^5 K hydrogen observed towards several nearby stars actually originate in the LB (Gry et al. 1995; Dupin & Gry 1998; Izmodenov et al. 1999).

Recent ROSAT soft X-ray observations have given rise to a new controversy about the LB hot gas. Shadows due to some clouds located outside of the LB have been observed in the 1/4 keV soft X-ray background, implying that a significant fraction of the observed X-ray emission is not emitted within the LB but originates in a more distant X-ray emitting hot gas possibly associated with the galactic bulge and halo (Moritz et al. 1998; Park et al. 1997). In addition, EUVE observations have led to a new upper limit for the EUV background intensity which significantly constrains the properties of the emitting gas (Jelinsky et al. 1995). The EUV data imply that either the gas is much cooler than 10^6 K, or that it is hot but at the same time it must be extremely metal deficient. In fact a new model that includes adiabatic cooling suggests that temperatures as low as 5×10^4 K could be characteristic of the LB gas, whereas classical models of supernova predict temperatures in excess of one million K (Breitschwerdt et al. 1996). The existence of the hot gas is also linked to the ionization state of diffuse clouds in the LB. The EUV spectra of white dwarfs imply a strong ionization of helium (stronger than that of hydrogen), in agreement with the ionization state of the circumsolar interstellar gas suggested by heliospheric observations (Lallement 1998). It is likely that the ionization of gas clouds in the LB could be due to an expanding shock that passed through the solar neighborhood less than one

million years ago (Lyu & Bruhweiler 1996), or it originates in X-ray emission from an interface between the hot (bubble) gas and diffuse clouds (Slavin 1998). However, we note that the second explanation is hardly compatible with the already 'cooled down' hot gas scenario.

Furthermore, a still unanswered question is the source of the strong difference between the pressure of the local interstellar cloud surrounding the Sun, as calculated from the confinement of the heliosphere (Lallement 1998), and the pressure of the hot interstellar gas within 100 pc as deduced from the diffuse EUV/soft X-ray emission measures (Berghoefer et al. 1998).

At present there are several opinions concerning the possible history of the structure of the LB that are somewhat contradictory. In one scenario the LB is thought to be an isolated supernova remnant cavity that has interacted with the adjacent Loop I superbubble, which is the volume bounded by the expanding shell associated with the cumulative stellar winds and supernovae explosions originating in the Sco-Cen OB association at a distance ~ 150 pc (Crawford 1991). In this model the Sun lies within the LB close to an annulus of compressed dense gas that separates the local hot gas from the 4 million degree gas filling Loop I (Egger & Aschenbach 1995). A second model describes the LB as a low density volume that has been sculpted in the ISM by stellar winds and supernovae explosions associated with the epochs of star formation in the Sco-Cen association over the past 15 million years (Breitschwerdt et al. 1996). Some authors have even questioned the actual existence of a real, isolated LB cavity surrounded by a wall of matter (Mebold et al. 1998).

In order to begin to answer some basic questions regarding the LB cavity Welsh et al. (1998), hereafter known as Paper I, have used the observed distribution of interstellar sodium (NaI) absorption within 250 pc of the Sun to infer the probable contours of neutral gas absorption in the local interstellar medium (LISM). Using absorption measurements towards 273 stars, contours of the LB (neutral) boundary were constructed to reveal a neutral gas-free cavity (presumably filled with hot LB gas) of radius 70 pc in most galactic directions, and extending to ~ 200 pc in one particularly low density direction (towards β CMa). This NaI survey of the LISM was carried out mainly using stellar targets of spectral type B with a visual magnitude brighter than V = 5.0, and hence due to the inherently limited number of directions sampled the very detailed contours of the neutral boundary ('wall') to the LB still remain uncertain, particularly in regions of high galactic latitude.

Recently the Hipparcos satellite (ESA 1997) has provided us with considerably improved stellar distance determinations for a large number of (fainter) A-type stars, and it is now possible to select many new targets with the aim of sampling more galactic lines-of-sight within 300 pc such that the absorption structure of the LISM, and in particular the neutral gas absorption boundary to the LB, can be diagnosed with far greater accuracy. Kinematic studies of the absorption properties of the local interstellar gas can clearly aid in defining the structure of the LB cavity. Such information can be gained from high resolution absorption spectroscopic observations towards nearby early-type stars, but thus far detailed observations have been performed for only several limited regions of the sky. While motions of the nearby gas (20 to 150 pc) from the fourth galactic quadrant have been interpreted as compression of the LB boundary by the expansion of the Sco-Cen/Loop I Bubble (Crawford 1991), the interstellar gas in the first galactic quadrant has apparently a far more complex kinematical structure (Genova et al. 1997), and the kinematics of the whole of the galactic anti-center hemisphere are still badly known. Clearly, more refined measurements of the location and velocity field of the dense (neutral) gas within the first 150 pc should provide meaningful constraints on the nature of the distribution of the hot gas (cavity) within the LISM, allowing us to provide greater constraints on current theoretical models of the LB.

In mid-1997 we started a long-term project of NaI absorption measurement lines-of-sight in the LISM using the Hipparcos distance data set. In this Paper we report on the preliminary findings of a sub-set of these high resolution NaI absorption observations towards 143 newly observed lines-of-sight. Combining these new results with some of the absorption data reported in Paper I (253 stars) and other recently published NaI data (60 stars), we present measurement of the D2-lines equivalent widths towards a grand total of 456 stars, which represents a 70% increase in the number of lines-of-sight previously sampled in the LISM. We believe, however, that the corresponding improvement in the contour definition is far greater than this value because we have gradually introduced interactivity in the target selection and observation process, i.e. when a target star has been observed and reveals a very small (or large) column density, it is easy to use lists of potential targets prepared in advance to select new targets at larger (or smaller) distances. Target selection was performed prior to, and also during the observing nights, and increases the efficiency of the search for the LB boundary. Using these new observations we have produced preliminary maps of the distribution of neutral sodium absorption out to a distance of 300 pc viewed using three different galactic projections. From these maps we have been able to better define the contour of the neutral absorption boundary to the LB cavity, and in addition these maps reveal both small and large-scale neutral interstellar gas features that may help in interpreting the past history of this region of galactic space.

2. Observations and data reduction

Observations of the two interstellar NaI D-lines at ~ 5890 Å were obtained on 3 observing runs between August 1997 and March 1998 using the echelle grating of the Aurelie spectrograph at the 1.52m telescope of the Observatoire de Haute Provence (France). Sight-lines were sampled using the criteria that stars possess: (i) a Hipparcos parallax π and an associated relative parallax error $\sigma(\pi)/\pi \leq 0.3$, (ii) a Hipparcos distance $\leq$ 300 pc, (iii) a spectral type earlier than A9V, and (iv) a rotational velocity $> 30\,\mathrm{km\,s^{-1}}$, and (v) preferentially a galactic position and a distance which help to fill gaps in the data presented in Paper I. Table 1 gives values for target HD numbers, galactic longitude and latitude, spectral type, magnitude and distance (in pc). These data were compiled using the SIMBAD data retrieval

Table 1. List of objects observed at OHP with their associated $W_\lambda(D2)_{m\text{Å}}$.

Star$_{HD}$	l	b	d(pc)	Sp. Type	V	$W_\lambda(D2)_{m\text{Å}}$	$W_\lambda(D1)_{m\text{Å}}$
1083	113.1	-34.9	126	A1Vn	6.35	4.4	<3.5
2913	114.5	-55.6	81	B9.5V	5.69	<3.5	<3.5
3240	120.7	-8.6	155	B7III	5.08	26.6	13.2
4636	122.5	-11.9	119	B9III	4.9	11.4	4.7
5267	124	-43.7	113	A1Vn	5.8	29.7	17
5394$^{(*)}$	123.6	-2.1	188	B0IVe	2.15	79.7	41.3
6658	126.1	-18.8	60	A3m	5.04	<3.5	<3.5
6811	126.1	-15.5	226	B7III	4.26	147.4	110.9
6829	124.7	6	97	A0Vnn	5.32	<3.5	<3.5
6960	125.1	1.4	126	B9.5V	5.56	22.7	12
7804	135.6	-58.6	67	A3V	5.13	<3.5	<3.5
10205	132.9	-21.3	209	B8III	4.96	56.4	31.7
10250	127.2	8.2	86	B9V	5.18	19.6	12.4
10390	134.5	-26.5	79	B9IV-V	5.63	6.2	<3.5
11291	132.6	-10.9	151	B9p...	5.7	37.5	24
11415	129.8	1.6	135	B2pvar	3.35	33.9	18.9
11946	130.2	2.7	79	A0Vn	5.29	<3.5	<3.5
18411	148	-16.9	100	A2Vn	4.68	<3.5	<3.5
18543	179.8	-51	98	A2IV	5.22	<3.5	<3.5
18633	179.7	-50.6	102	B9.5V	5.56	<3.5	<3.5
20150	162.4	-30.6	104	A1V	4.87	<3.5	<3.5
21427	141.9	2.5	103	A2V	6.14	<3.5	<3.5
23850$^{(*)}$	167	-23.2	117	B8III	3.62	70.1	59.8
26677	183.9	-29.2	93	A2m	6.52	<3.5	<3.5
26912$^{(*)}$	184.2	-28.9	133	B3IV	4.27	125.7	115.3
27638	171.5	-16.7	82	B9V	5.38	5.3	<3.5
27820	185.1	-26.9	122	A3V	5.1	41.4	31.5
28149	174.3	-17.7	127	B7V	5.53	65.5	47.5
29459	174.4	-14.1	111	A5Vn	6.21	39.8	19.6
29646	172	-11.6	103	A2V	5.73	6.4	3.5
32608	169.5	-3	82	A5V	6.49	25.4	13.7
32630	165.4	0.3	67	B3V	3.18	4.7	<3.5
34203	191.3	-15.3	113	A0V	5.52	32.3	20
34452	172.9	-2.1	137	A0p...	5.38	12.1	7
34904	167.3	2.6	92	A3V	5.54	57	39.3
36162	189.7	-10.2	106	A3Vn	5.93	63.8	44.7
36777	200.4	-15.3	106	A2V	5.32	4.4	<3.5
38545	192.6	-7.1	130	A3Vn	5.72	34.1	16.4
39662	195.9	-7	94	A2V	6.59	<3.5	<3.5
40312	174.3	6.7	53	A0psi	2.65	<3.5	<3.5
42824	210.7	-9.7	145	A2V	6.62	18	8
43812	155.4	19.5	129	A3V	6.05	6	<3.5
44472	144.1	23.6	170	A4V	6.03	9.5	6.3
45105	167.4	15.9	96	A0V	6.55	18.2	6.8
45380	216.9	-8.9	125	A0Vn	6.35	<3.5	<3.5
45542	192.4	4.3	154	B6III	4.13	80	43.3
45720	174.8	13.3	164	A0	6.66	126.9	90.5
46089	200.4	1	65	A3V	5.22	<3.5	4
46590	158.6	20.6	99	A2V	5.87	9.6	7
50973	171.6	19.9	69	A2Vn	4.9	<3.5	<3.5
54801	190.5	16	120	A4IV	5.75	24.7	17.3
56221	177.1	22.1	82	A5Vn	5.87	<3.5	<3.5
57103	162	26.4	144	B8V	5.8	98.7	63.4
57744	195.4	17	96	A1V	6.17	18.3	9.9
59169	261.4	-15.1	118	G3IV/V	9.86	13.6	7
60107	203.2	16.3	115	A1Vn	5.27	19	9.4
61497	158.5	29.5	73	A3IVn	4.93	13.6	8
63586	162.7	30.6	135	A0Vn	6.36	<3.5	<3.5
66824	176.8	31.5	145	A1V	6.35	29	15
71150	196.6	31.8	85	A3V+...	6.3	<3.5	<3.5
72359	215.3	27	166	A1V	6.48	113.7	84.6
72524	186	35.6	98	A2Vnn	5.76	24.6	18
74521	216.7	29.7	125	A1p...	5.63	<3.5	<3.5
89774	224.5	53.2	146	A1V	6.16	139.7	116.7
91636	236.3	52.9	142	A2V	5.67	42.7	27.4
96738	213.3	66.8	125	A3IV	5.7	<3.5	<3.5
100740	251.6	65.9	122	A4Vn	6.57	<3.5	<3.5
104321	270.3	66.2	109	A5V	4.65	<3.5	<3.5
107655	231	83	100	A0V	6.21	<3.5	<3.5
111133	299.9	68.8	161	A0spe...	6.31	<3.5	<3.5
111308	299.6	76.4	125	A1V	6.47	<3.5	<3.5
111421	124.2	68.7	142	A6m	6.25	5.6	<3.5
113865	64.1	86.2	108	A3IV	6.51	<3.5	<3.5
115995	320.3	64.8	125	A3V	6.26	10.8	7
119537	326.1	55	127	A1V	6.51	141.5	111.5
121996	17	73.8	147	A0Vs	5.76	18.1	8.9
124931	340.3	53.4	166	A1V	6.15	37.3	23
130557	353	50.2	108	B9Vsvar...	6.15	16.4	9.5
132742	348.9	42.5	93	B9.5V	4.91	15.4	7
138764	356.1	36.4	107	B6IV	5.16	90.2	55.2
141851	5.2	37.2	49	A3Vn	5.09	<3.5	<3.5
145607	3.9	29.7	77	A4V	5.43	$\sim 30^{(!)}$	$\sim 15^{(!)}$
145622	110.9	35.4	178	A3V	5.73	16.2	7
145876	8.3	32.2	84	A5	6.96	<3.5	<3.5
148207	17	33.1	113	A0	6.66	37.4	20.7
148857$^{(*)}$	17.1	31.8	51	A2V	3.82	<3.5	<3.5
149911	10	25.7	126	A0pe...	6.05	108	97.1
150378	20.8	30.9	93	A1V	5.77	19.8	10.8
151862	31.5	32.9	88	A1V	5.91	7.1	<3.5
154145	19.7	23.7	95	A2	6.7	57.4	32.2
154445	19.3	22.9	235	B1V	5.63	215	176.7
154895	19.5	22.3	83	A3V	6.06	91.1	64.6
155103	59.3	35.6	54	A5m	5.41	<3.5	<3.5
156247$^{(*)}$	22.7	21.6	186	B5Vnn	5.89	168.6	141.9
156729	61.3	33.9	55	A2V	4.64	<3.5	<3.5
159139	52.1	28.9	84	A1V	5.66	7.5	<3.5
159170	18.6	14.5	48	A5V	5.61	12.5	$<6^{(!)}$
161693	81.5	31.4	127	A2V	5.75	46.1	32.2
162579	78.1	30.3	67	A2V	5.02	7.18	<3.5
164577	28.4	11.6	81	A2Vn	4.42	57.8	36.6
169702	67.3	21.8	135	A3IVn	5.11	23.5	13
170000	101.9	28	89	A0p(Si)	4.22	<3.5	<3.5
170073	87.9	26.4	58	A3V	4.98	<3.5	<3.5
171301	59	17.1	112	B8IV	5.47	39.1	34
174262	50	9.2	86	A1V	5.89	$<6^{(!)}$	<3.5
174602	62.4	14.5	73	A3V	5.22	<3.5	<3.5
178207	83.8	19.6	107	A0Vn	5.4	<3.5	<3.5
180317	54.5	4.5	97	A4V	5.65	47.3	35.7
187235$^{(*)}$	73	6.6	150	B8Vn	5.83	43.4	25
187362	56.5	-3.4	100	A3V	5.01	<3.5	<3.5
188350	40.5	-13.9	106	A0III	5.6	217.9	192.6
193369	75	0.6	60	A2V	5.58	9	4.8
193472	55.6	-12.7	90	A5m	5.96	8.5	4
195050	77.3	0	83	A3V	5.63	16.2	6.6
196180	58.6	-15.2	70	A3V	4.64	<3.5	<3.5
196740	67	-10.3	151	B5IV	5.06	13.5	5.8
198069	52.8	-22.5	157	A0V	5.57	34.6	14.5
199254	59.8	-20.4	61	A4V	5.54	<3.5	<3.5
201908	112.4	20.2	126	B8Vn	5.91	<3.5	<3.5
203535	89.9	-2.2	89	A2	6.73	<3.5	<3.5
204414	77	-16.6	56	A1V	5.39	<3.5	<3.5
205314	93.6	-1.2	146	A0V	5.77	<3.5	<3.5
205835	87.6	-8.8	63	A5V	5.04	<3.5	<3.5
206774	87.1	-11.2	84	A0V	5.69	33	16.3
209409$^{(*)}$	57.4	-42.7	117	B7IVe	4.74	103.2	83.7
209833	84.5	-21.3	93	B9Vn	5.69	28.7	16.3
211211	94.8	-11.2	86	A2Vnn	5.72	100.6	81
212710	120.2	24.1	78	B9.5Vn	5.27	<3.5	<3.5
213323	91.3	-21.5	125	B9.5V	5.64	127.6	84.4
213660	95.9	-15.7	193	A6V	5.88	134.5	108.9
214546	72.5	-45	88	A3	6.82	$30^{(!)}$	25
214734	108.8	4.4	98	A3IV	5.19	<3.5	<3.5
216735	80.8	-44.3	87	A1V	4.91	45.3	26.2
216831	98.3	-20.9	256	B7III	5.73	185.7	157.7
220061	97.5	-34.6	51	A5V	4.58	<3.5	<3.5
220599	102.5	-27	155	B9III	5.56	52.8	33.5
221253	112.5	-2.7	176	B3IV	4.89	142.2	122.1
222304	111.3	-10.8	120	B9V	5.35	<3.5	<3.5
222602	94.4	-51.7	104	A3Vn	5.89	131.1	100.5
222922	110.4	-17.5	152	A0	6.93	28.8	15.1
223274	117	5.7	91	A1Vn	5.05	22.2	14
223386	115.2	-1.9	105	A0V	6.33	9.6	4.6
223438	92.6	-58.1	82	A5m	5.77	32.6	20.2

Note: (*) Redundant observations with Paper I.
(!) Low S/N – Measurement uncertain.

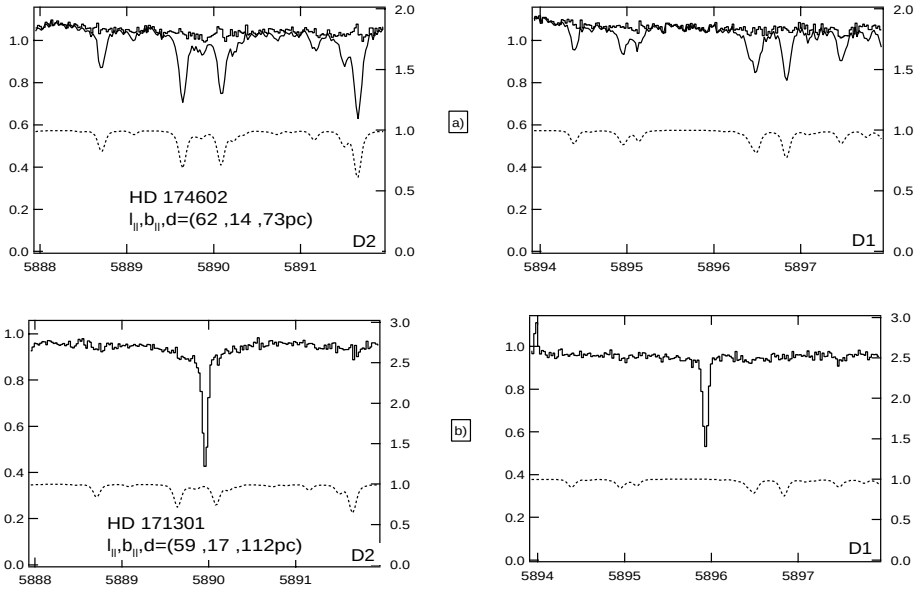

Fig. 1. Plots of the D2 and D1 absorption raw spectra (solid line); computed synthetic spectrum used for telluric absorption correction (dash line); remaining water corrected stellar spectrum (bold). Plot 1(a) HD174602, 1(b) HD171301.

system of the Astronomical Data center in Strasbourg(France) and the on-line Hipparcos catalog (ESA 1997).

The spectral resolution of the interstellar observations was checked against that of a Th-Ar calibration lamp, resulting in R = 100,000 ($3\,\mathrm{km\,s^{-1}}$). All spectra were well exposed with signal-to-noise ratios typically in excess of 30.

The data were reduced using IGOR (Wave Metrics) software routines that account for the division by a flatfield and background light subtraction. The numerous telluric water vapor lines that contaminate the spectra around the NaI lines were removed using a computed synthetic atmospheric transmission spectrum described in Lallement et al. (1993) which is automatically performed by a single routine created in the context of the IGOR Software. Synthetic spectra are calculated according to a spectroscopic data bank, adjusted for the specific observation (i.e. altitude of the observer, amount of atmospheric water vapor absorption), and convolved with the instrument profile to finally divide the stellar spectrum by the computed telluric absorbing profile.

Since the rest wavelengths of the numerous telluric lines are very accurately known, these were used to establish a wavelength scale (accurate to $\pm\,0.2\,\mathrm{km\,s^{-1}}$), which was subsequently corrected to produce heliocentric wavelengths. The resultant spectra were then fitted with a high order polynomial to establish a local stellar continuum level. The equivalent widths (W_λ) of the D2 and D1 lines were then measured and their values listed in Table 1. Typical errors on the measured (W_λ) were $\pm$ 5%. Although we report only the NaI equivalent widths in this preliminary paper, subsequent papers will present the individual gas cloud component column densities and velocities obtained from detailed fitting of these interstellar absorption line profiles.

As an indication of the quality of the recorded spectra and the efficacy of the telluric line removal process, in Fig. 1a we show the raw D2 and D1 absorption spectra recorded towards the star HD 174602, together with the computed synthetic spectrum used for telluric absorption correction of the raw data. After division by this synthetic spectrum we show the remaining stellar spectrum that reveals no detectable interstellar D2 and D1 absorption lines. In contrast to this situation, in Fig. 1b we show the strong interstellar D2 and D1 lines observed towards the star HD 171301, with D2 and D1 equivalent widths respectively equal to 39 and 34 mÅ. We have made conservative estimates of the strength of a potential absorption feature for a typical target showing no absorption line at a level of greater than 2σ above the rms value of the local continuum, at a position $\pm\,50\,\mathrm{km}\,s^{-1}$ from the rest wavelength of the D2 or D1 lines. For a typical observation (such as HD174602) in which telluric contamination is not severe, this resulted in an equivalent width detection upper limit of < 3.5 mÅ for the D2 line.

The resultant interstellar NaI profiles for the remainder of our target stars will be presented (together with their profile fit parameters) in a future publication (Sfeir 2000)

3. Other published data

In order to maximize the number of line-of-sight measurements of NaI in the LISM, we have added the following NaI absorption data to our present sample: (a) we have included NaI D2-line equivalent widths towards 253 lines-of-sight from Paper I, and (b) we have added the NaI equivalent width data listed in Table 2 which is a compilation of high resolution absorption measurements towards 60 stars that have been published in the literature subsequent to those listed in Paper I. Our selection of these additional lines-of-sight is restricted to those stars with a Hipparcos distances $\leq$ 300pc and $\sigma(\pi)/\pi \leq 0.30$.

In order to assign values for lines-of-sight to stars that have only NaI column density and no corresponding NaI D2 equivalent width, W_λ (D2), reported in the literature, we have constructed an "empirical" curve-of-growth using the NaI measurements for a sample of 440 stars as presented in Penprase (1993) and Welsh et al. (1994). For lines-of-sight with W_λ(D2) < 20 mÅ (i.e. log N(NaI) $< 11.1\,\mathrm{cm^{-2}}$ where N(NaI) is the to-

Table 2. Other published NaI observations post Paper I.

Star$_{HD}$	Name	l	b	d(pc)	W$_\lambda$(D2)	W$_\lambda$(D1)	logN$_{(NaI)TOT}$	Ref.
–	BD+471474	171.7	27.6	163	125	98	>12	(9)
6882	ζ Phe	297.8	–61.7	86	<4.5	–	<10.39	(1)[a,c]
10144	α Eri	290.8	–58.8	44	<2.4	–	<10.11	(1)[a,c]
14034	–	195	–69	201	110	81	>11.9	(9)
14139	–	188.7	–67.4	101	<10	<10	<10.7	(9)
14256	–	190.1	–67.5	142	29	20	11.3	(9)
14613	–	191.8	–67	121	129	122	>12.08	(9)
14670	–	191.6	–66.8	116	55	52	11.7	(9)
22252	–	282.2	–43.7	261	>483	–	13.04	(9)[a]
22449	–	290.4	–38.4	151	<3.7	–	<10.30	(8)[a]
22488	–	282.3	–43.4	207	167	–	12.57	(8)[a]
22634	–	281.1	–43.8	110	<3.7	–	<10.30	(8)[a]
23509	–	281.4	–42.8	214	>483	–	13.17	(8)[a]
25938	–	285.2	–38.8	101	145.2	–	12.45	(8)[a]
26109	–	284.1	–39.1	234	129	–	12.37	(8)[a]
26594	–	287.2	–37.3	229	225	–	12.77	(8)[a]
29769	–	285.3	–35.7	148	87.4	–	12.04	(8)[a]
34085	β Ori	209.2	–25.2	237	50.1	–	11.6	(1)[a]
36486	δ Ori	203.9	–17.7	281	70.4	42.6	–	(6)[b]
37742	ζ Ori	206.5	–16.6	251	164.7	137.1	–	(6)[b]
38771	κ Ori	214.5	–18.5	221	149.3	117.5	–	(6)[b]
58520	–	171.7	25.4	114	<5	<5	<10.7	(9)
59975	–	170.1	26.8	214	72	70	11.82	(9)
60653	–	173.7	26.7	223	145	121	>12.08	(9)
65575	χ Car	266.7	–12.3	119	<3	–	10.2	(1)[a,c]
74575	α Pyx	255	5.8	259	75.7	–	11.92	(1)[a]
101075	–	135.5	51.1	237	227	190	–	(2)
102355	–	136	54.1	114	31	15.2	–	(2)
107273	–	129.3	54.4	184	11.2	6.5	–	(2)
112091	μ^2Cru	303.4	5.7	111	62.9	–	11.77	(4)[a]
112092	μ^1Cru	303.4	5.7	116	49.4	–	11.59	(4)[a]
118716	ϵ Cen	310.2	8.7	115	<3	–	<10.2	(1)[a,c]
140873	25 Ser	5.5	39	125	139.3	120	–	(5)
141569	–	4.2	36.9	99	188	–	12.65	(3)[a]
142630	–	341.3	14.8	60	6.4	2.2	–	(5)
144708	11 Sco	359.4	27.9	131	160.8	140	–	(5)
144844	–	350.7	20.4	131	165	146.7	–	(5)
145482	13 Sco	348.1	16.8	143	40.4	23.5	–	(5)
145502	μ Sco	354.6	22.7	134	235.4	201.9	–	(5)
147971	ϵ Nor	336	1	123	225	–	12.76	(1)[a]
150462	–	57.7	41.2	177	15.5	–	11	(8)[a]
151749	–	60.6	39.9	154	73.9	–	11.9	(8)[a]
153613	–	352	6	151	12.3	7.1	–	(5)
157841	–	16.8	15.7	175	>483	–	13.8	(3)[a]
157955	–	357.2	2.9	184	181.6	168.6	–	(5)
159532	θ Sco	347.1	–6	83	68.8	41.4	–	(6)[b]
172910	–	359.8	–14.1	138	62.3	63.8	–	(5)
178125	18 Aql	44.5	1.6	156	83.2	68.7	–	(5)
180555	–	48.7	1.2	114	84	58.4	–	(5)
181440	27 Aql	35.5	–6.9	156	92	70.6	–	(5)
183914	β CygB	62.1	4.6	115	33.3	17.5	–	(5)
184597	–	6.8	–23.1	265	184	–	12.62	(7)[a]
184606	9 Vul	55.4	–0.1	187	76.3	43.9	–	(5)
186417	–	9.3	–24.4	234	101.5	–	12.17	(7)[a]
186500	–	8.3	–24.8	167	145.6	–	12.46	(7)[a]
189090	11 Sge	55.5	–6.4	124	7.6	3.8	–	(5)
189395	–	67.8	0.8	167	26.4	15.4	–	(5)
193924	α Pav	340.9	–35.2	56	<2.2	–	<10.07	(1)[a]
195554	–	91.9	9.9	275	54.8	32.4	–	(5)
196504	27 Vul	68.7	–8.7	94	35.2	23.9	–	(5)

[a] W$_\lambda(D2)$ derived from N$_{(NaI)TOT}$;
[b] W$_\lambda(D2)$ derived from W$_\lambda(D1)$;
[c] Redundant observations *with Paper I*
References: (1) Welsh et al. (1997); (2) Benjamin et al. (1996); (3) Sahu et al. (1998); (4) Meyer & Blades (1996); (5) Genova et al. (1997); (6) Welty et al. (1994); (7) Lyons et al. (1994); (8) Penprase et al. (1998); (9) Grant & Burrows (1999)

tal column density of NaI absorption) we have checked that this part is indeed best fit with the linear part of the curve-of-growth. For 11.1 cm^{-2} < log N(NaI) < 13.0 cm^{-2} (i.e. 20 < W$_\lambda$(D2)) < 480 mÅ) the empirical data is best fit with a theoretical temperature of 10,000 K. This high temperature is due to the presence of multiple absorption components that cause the inherent width of the NaI line to be overestimated. From this empirical curve we read off values for the D2 equivalent width when only the value of N(NaI) is reported. In the same way, we have constructed an empirical curve of W$_\lambda$(D2) vs W$_\lambda$(D1) from the measurements, checked that this curve is best fit with the theoretical curve for T=10,000 K, and we read off values

for the D2 equivalent width when only the value of the D1 equivalent width is reported. Finally, for the few cases of highly saturated lines-of-sight with reported values of log N(NaI) $>$ 13.0 cm^{-2} or W$_\lambda$(D1) $>$ 220 mÅ,we have assumed W$_\lambda$(D2) $>$ 480 mÅ and W$_\lambda$(D2) $>$ 240 mÅ respectively.

4. Discussion

The major long-term aim of our program of observations is to map the detailed distribution and kinematics of neutral interstellar gas within 300 pc. The evacuated Local Bubble region should thus appear as a cavity in the distribution of the (denser) neutral gas of the surrounding galactic ISM. We assume that absorption due to the NaI ion is a good indicator of the total amount of neutral interstellar gas in a particular line-of-sight. This assumption is reasonable since NaI generally resides in "cold" (T $<$ 1000 K) and predominantly neutral interstellar regions (Hobbs 1978). In addition, it has been shown that N(NaI) is well correlated with the total column density of neutral hydrogen, N(H), for values of log N(NaI) $>$ 11.0 cm^{-2} (Welty et al. 1994; Ferlet et al. 1985). This range of NaI column density (corresponding to a D2-line equivalent width of $>$ 20 mÅ) is typical of interstellar gas with a neutral hydrogen column density of log N(HI) $>$ 19.3 cm^{-2}, and is representative of the lowest column density found in interstellar clouds of the cold, neutral medium described in the standard model of the ISM (McKee & Ostriker 1977). Such clouds typically have a gas density of $>$ 1 cm^{-3} and a temperature of $<$ 100 K.

4.1. Density – distance plots

A simple understanding of the gross characteristics of interstellar neutral absorption in the LISM can be gained from a plot of the level of NaI absorption (i.e. W$_\lambda$(D2)) versus distance in pc to the background stellar source. This dependence is shown in Fig. 2 and we can immediately see that little measurable NaI absorption is detected for distances (in all galactic directions) up to $\sim$ 75 pc. Infact, from all 84 lines-of-sight sampled with distances less than 70 pc, we have detected only 3 stars (δ Cyg, 2 Cet and HD 129685) with a value of W$_\lambda$(D2) $>$ 15 mÅ. This paucity of detectable neutral NaI absorption for distances $<$ 70 pc is clear evidence for the existence of a neutral gas-free cavity (i.e. the Local Bubble).

Although Fig. 2 is helpful in confirming the existence of the local void, in order to obtain a better insight into the actual 3-D structure of the LB we need to produce contours of the D2-line absorption strength as a function of galactic coordinates. To derive different galactic views of the neutral absorption characteristics of the LISM we have produced contours of the D2-line equivalent width as a function of the stellar galactic coordinates projected onto three different galactic planes of reference. Each of these projections contain the Sun at the center and are defined as follows: (a) a (downward) view of the galactic plane, (b) a view perpendicular to the galactic plane that contains both galactic poles and the galactic center, or a view in the local galactic meridian plane, (c) a view perpendicular to both views

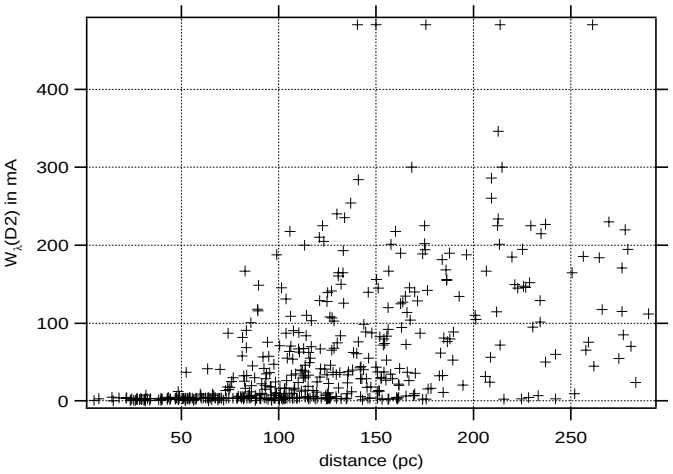

Fig. 2. Plot of D2 equivalent width (mÅ) versus d(pc) for all target stars in our database.

(a) and (b) that contains both galactic poles and is perpendicular to the galactic center direction (i.e.the galactic rotation plane). In all the plots we use a spherical projection, i.e. the Sun-star distance in the figure is the real distance irrespective of the angle above or below the reference plane. In order to reduce projection errors, only stars whose line-of-sight are less than 18° above (or under) the plane of reference were selected. We have found that selection by angle is the best compromise to produce a large enough sample of selected stars and at the same time minimizing the variations in projection effects. Selection according to the distance from the projection plane (i.e. stars selected within a slab of limited thickness) revealed drawbacks for very nearby stars with large angular offsets from the reference plane and for very distant stars that would have been useful for defining the outer contours of the LB ("edge effects"). In future papers as our total number of lines-of-sight increases we shall be able to produce alternative plots based on new projection selection criteria.

We have developed a code in the context of the IGOR software which, after selecting stellar targets with the appropriate galactic projection criteria, uses the Delaunay triangulation to interpolate the positions of a specified contour trace from the equivalent width values at each projected star position. In general we have used 16 iterations of the interpolation process to get smooth contours within a reasonable computation time-scale. Fig. 3, 4, 5 show the resulting Na-D2 equivalent width absorption contours at 5, 10, 20, and 50 mÅ. As stated earlier, a D2-line equivalent width of 20 mÅ corresponds to a neutral hydrogen column density of log N(HI) $\sim$ 19.3 cm^{-2}, and is sufficient to provide an optical depth of $\sim$ 4.1 to a 200 Å EUV photon. This amount of absorbing neutral gas would result in the emitted flux from an EUV source being attenuated by almost 99%, thus essentially defining the viewing horizon for most EUV sources. This absorption plotting level was used in Paper I to define a plausible LB boundary, and hence a direct comparison between our new results can be made.

For soft X-ray 1/4 keV photons that are assumed to originate in a 1 million degree K plasma, unit optical depth is achieved with a neutral hydrogen column density of N(HI) = 10^{20} cm^{-2}. This corresponds to a saturated D2-line with an equivalent width of $>$ 50mÅ,and thus this plotting contour could well define the limit of the contribution of the soft X-ray background radiation originating in a hot LB region (see Sect. 4.5).

The method of using automatic iso-contours has some limitations, since in some regions the number of neighbouring target stars used for the triangulation calculation is not optimal and the contours are not well constrained. Additionally, in order to aid in the reader's interpretation of the present isocontours, markers for the target stars in Fig. 3, 4 and 5 are represented by two sets of triangles whose plotted size increases with the angle (i.e. 0–9° and 9 - 18°) between the target and the reference plane. Also, the shape of the triangle (up- or down- oriented) reflects the location (above or below) the plane. This quasi 3-dimensional representation allows easier recognition of which gaseous condensations are responsible for the derived contours. It should be recognized that due to the limited number of targets presently available in any particular sight-line and the fact that the interpolation calculation uses targets with an angular spread of up to $\pm$ 18° the very detailed variation of the derived LB contours must be viewed with some caution. In subsequent papers as our number of target stars increases, and thus their angular spread decreases, the confidence level of the derived isocontours will be greater.

4.2. The LISM viewed from above the galactic plane – Fig. 3

Fig. 3 clearly shows a large region surrounding the Sun in the galactic plane that is deficient in neutral interstellar NaI gas absorption. Without a local void, the 50 mÅ isocontours would be 5 times more distant than the 10 mÅ isocontours, which is clearly not the case in Fig. 3. Where sufficient measurements exist, the contours of the strength of the D2-line increases from an absorption level of 5 mÅ to 20 mÅ over a distance of only $\sim$ 25 pc. In most lines of sight, a D2-line equivalent width of $>$ 50 mÅ is reached after a further 30 pc. This rapid increase in absorption confirms the existence of a build-up or "wall" of neutral gas that surrounds the central regions of the LB void. Additional evidence for a overall sharp build-up in neutral absorption strength can be seen in Fig. 2, in which there is an appreciable increase in the measured equivalent widths for most stars with distances $>$ 75 pc.

This void of neutral gas absorption (which we identify as the LB) is clearly asymmetric, with a minimum radius of $\sim$ 60 pc in the direction of galactic longitude l = 0° (towards the Galactic Center) and a maximum extension $>$ 200 pc in the l = 235° direction (towards the star β CMa). More specifically, the closest approach of the proposed LB neutral boundary in the galactic plane is towards the direction of l = 30° (towards Ophiuchus), consistent with the intersection of the X-ray deficient Egger Ring feature and the galactic plane (Egger & Aschenbach 1995). We also note the confirmation of an interstellar "tunnel" that bulges in extent to a distance of $\sim$ 160 pc in the galactic direction of l = 330° $b \sim 12$ ° (towards Lupus-Norma) as first suggested by Welsh et al. (1994). We note that the entire region between l = 300° - 350° (i.e. Sco-Cen-Lup) which corresponds to the central area in the middle of the Egger Ring feature, is indeed very clumpy.

Fig. 3 reveals a single, relatively "dense" accumulation of neutral gas within 60 pc of the Sun (l = 80°) which lies close to the galactic plane (confirmation of this feature can be found in an alternate view of the LB shown in Fig. 5. This small patch of denser gas is observed towards the star δ Cyg (d = 52 pc), and has a column density value of log N(NaI) = 11.43 cm^{-2}. Using the ultra-high resolution data of of Welty et al. (1996), we derive a N(NaI)/N(CaII) ratio of 5.2 for this sight line. This ratio is at least an order of magnitude greater than that commonly found for the local "fluff" gas clouds residing in the LISM (Bertin et al. 1993), and the derived NaI doppler width parameter of 0.42 km s^{-1} indicates a gas cloud temperature of $<$ 220 K (Hobbs and Welty 1991). The existence (and survival) of such cold gas within the hot, ionized surroundings of the LB is difficult to explain and clearly merits further observations.

We note a similar (larger) accumulation of dense neutral gas lying within the LB cavity at a distance of $\sim$ 85 pc in the direction of galactic longitude l = 95° (towards HD 211211) lying 11° below the galactic plane. There are also several small regions of high (and low) levels of NaI absorption lying at distances $>$ 100 pc in many galactic directions revealed by Fig. 3 that clearly require further observation to refine their relationship with the presently derived LB contour boundary.

The extension of the very low density neutral cavity in the direction of the star β CMa has been well documented (Gry et al. 1985; Welsh 1991). Although there is sparse NaI data for lines-of-sight beyond a distance of $\sim$ 200 pc that accurately defines the contour of the LB extension in this direction (i.e. $l \sim$ 240°), we note that the star κ CMa (d = 242 pc) has a low column density of log N(NaI) $<$ 10.18 cm^{-2} whereas both γ Col (d = 262 pc) and ω CMa (d = 283 pc) have higher column densities of log N(NaI) $>$ 11.0 cm^{-2} along a similar line-of-sight (Welsh et al. 1994). Thus, the data suggest that the β CMa tunnel is fully absorption bounded (to a level of 50 mÅ) at a distance of $\sim$ 250 pc, or that it is bounded at a closer distance with some quite narrow interstellar holes in the absorption boundary. Recently Heiles (1998), using HI, IR and radio contiuum data, has found evidence for a new superbubble centered at a distance of $\sim$ 800 pc which is purported to be intersecting with our own LB in the galactic direction of l = 230°. Our data do not support Heiles' idea that both bubbles have merged into one large elongated cavity, but instead we favor the notion that Heiles' new superbubble is a separate entity with a maximum radius of $\sim$ 500 pc.

Our present data may also explain the difference of a factor of $\sim$ 10 in the observed total neutral + ionized hydrogen column density between the two near neighbor stars β and ϵ CMa (Dupin & Gry 1998). Inspection of Fig. 3 shows that ϵ CMa (d = 132 pc) is placed within the contours of the LB, at large distance from the real "wall" represented by the 20 and 50 mÅcontours and thus presumably resides within a region of hot, ionized LB

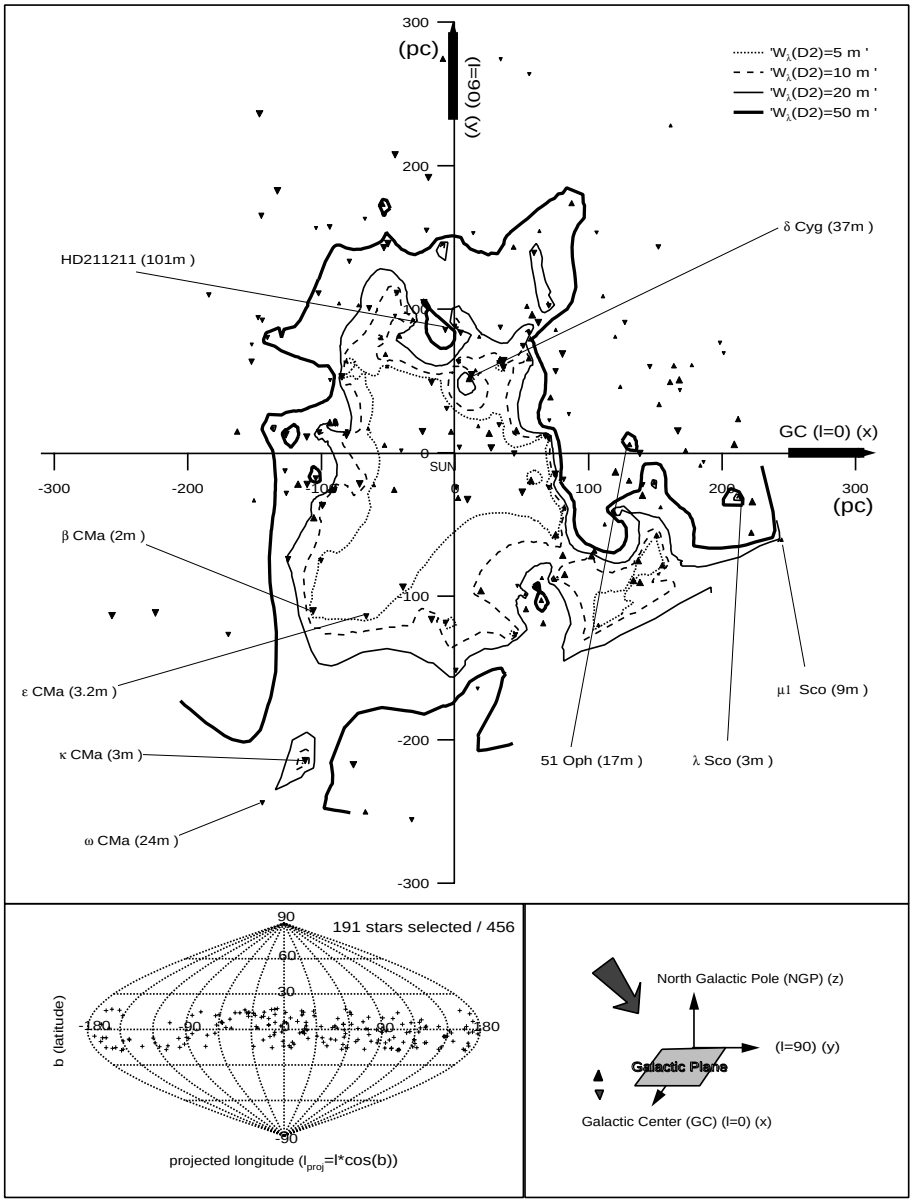

Fig. 3. Derived D2 absorption contours at 5, 10, 20 and 50mÅ(m is for mÅ) for stars (represented on the plot as triangles) projected onto the Galactic Plane. We also show the galactic distribution of the 191 stars selected and a pictorial representation of the projection used.

gas. We note that this is consistent with the absence of neutral interstellar HeI observed towards this star by Cassinelli et al. (1995). Alternately, β CMa (d = 153 pc) is positioned closer to (or perhaps just within) the LB neutral wall boundary and thus the large ionized gas column density noted by Gry et al. 1985 is probably due to the ionized precursor sheet at the LB wall interface. This is entirely consistent with the EUV spectrum of β CMa which requires a large interstellar neutral HeI column density to fit the observed data (Cassinelli et al. 1996). The EUV data imply that there is an interstellar cloud component towards β CMa (which is not seen towards ϵ CMa) that contains appreciable amounts of neutral helium. However, we note that this component has a low HI:HeI ratio, implying that the cloud is ionized by a different process than the LB gas. The recent ultraviolet absorption spectrum of β CMa is, again, consistent with this argument (Dupin & Gry 1998).

4.3. The LISM in the meridian plane – Fig. 4

This view of the LISM viewed at right angles to the galactic plane shows that the LB is "wasp-waisted" with significant elongations towards both galactic poles. We note that the two narrowings are almost diametrically opposite each other, offset respectively by $\sim 20^\circ$ above and below the galactic plane (i.e. the approximate plane of Gould's Belt). The narrowing in the general direction of the galactic center is probably due to denser gas associated with both the Ophiuchus Complex and the Sco-Cen association (i.e. Loop I), and the narrowing towards the anti-center direction is due to denser gas associated with the Perseus-Taurus clusters. Crawford (1991) and Genova et al. (1997) have found a general outflow of neutral gas from the expanding Sco-Cen association, consistent with our present picture of the LB possibly being "squeezed" from opposite sides of the galactic plane. Verification of this scenario will have to

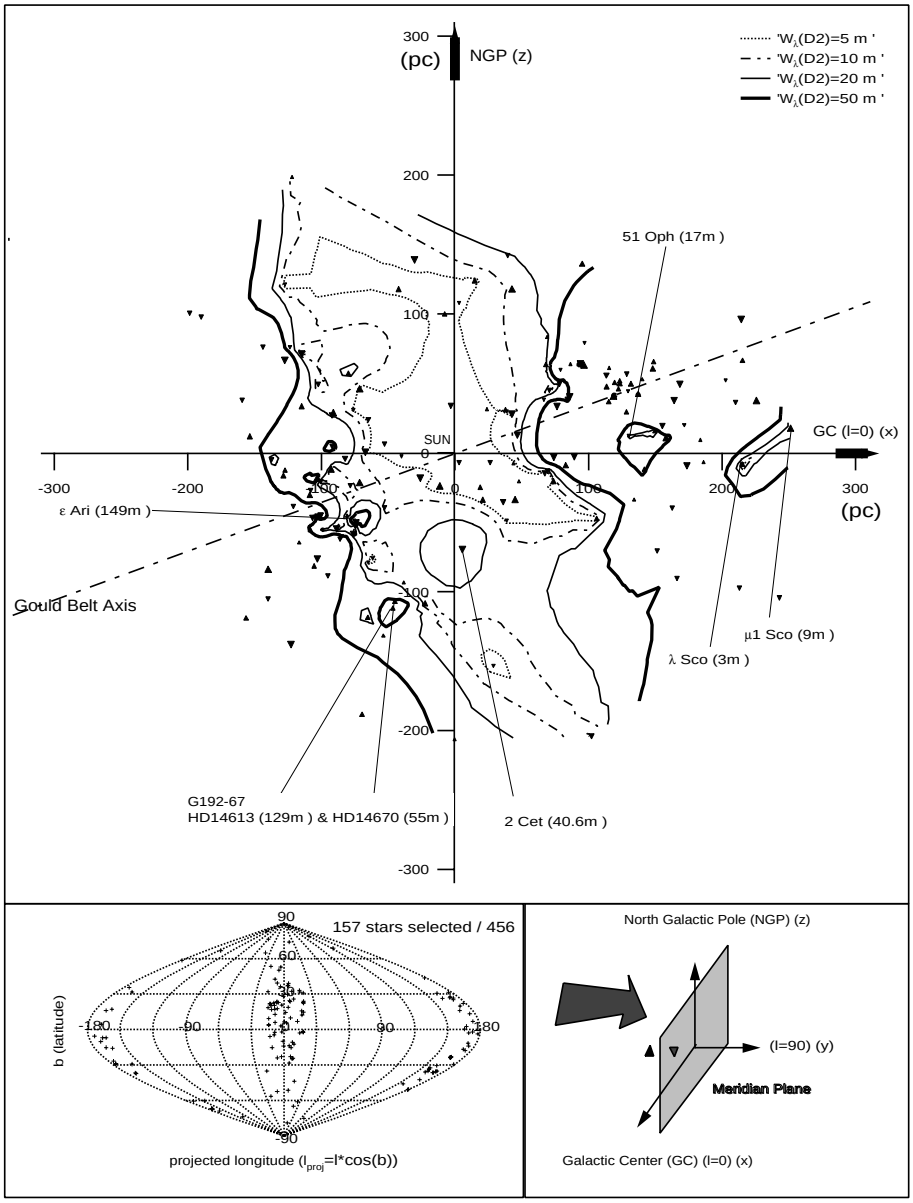

Fig. 4. Derived D2 absorption contours at 5, 10, 20 and 50 mÅ(m is for mÅ) for stars (represented on the plot as triangles) projected onto the Meridian Plane. We also show the galactic distribution of the 157 stars selected and a pictorial representation of the projection used.

wait until we obtain information on the kinematics of the neutral absorbing wall of interstellar gas derived from profile fitting of all the NaI data. However, our preliminary contour data do support the view that the LB is a neutral void whose shape is defined by the intersecting absorption boundaries of large, more distant galactic supershell structures as suggested by Welsh et al. (1994).

We note one noticeable condensation of neutral gas within the central LB cavity at $l = 72°$ at a distance of ~ 70 pc below the galactic plane (along the axis towards the South Galactic pole) due to an interstellar cloud surrounding the star 2 Cet. A doppler width parameter of 8.5 km s^{-1} is required to fit the NaI data for 2 Cet (taken at a spectral resolution of 5 km s^{-1}) as presented in Welsh et al. (1994). It seems likely therefore, even allowing for the presence of unresolved NaI components, that this gas is warm and probably partially ionized. This is in contrast to the neutral "globule" surrounding δ Cyg discussed earlier and the line-of-sight to 2 Cet clearly merits further study using higher ionization ions.

Another noticeable feature of Fig. 4 is the very clumpy nature of the LB wall towards the galactic anti-center (towards Perseus-Taurus). There are several small, but quite dense condensations of NaI gas residing within the general 20–50 mÅ contours throughout this region. One of these dense complexes of NaI is seen towards the star ϵ Ari (l = 159 °) at a distance of 90 pc below the galactic plane. This neutral gas is associated with the MBM 12 molecular cloud complex, which is thought to be the nearest molecular cloud to the Sun, and was previously thought to lie within the hot LB (Hobbs et al. 1986). Close inspection of Fig. 4 shows this complex of neutral gas clouds to be located within the LB neutral wall at the very edge of the outer LB contour. The observed ratio of N(NaI)/N(CaII) = 5 towards ϵ Ari confirms its association with cold, neutral interstellar gas (presumably due to dense neutral gas of the LB wall boundary),

rather than the warm, partially ionized diffuse "fluff" gas scattered within the LB. The placement of the MBM 12 clouds just outside (or at the very edge of) the LB has great importance for the interpretation of the all-sky maps of soft X-ray background emission, and will be discussed in detail in Sect. 4.5. Similarly, the dense gas seen towards HD 14613 and HD 14670 (d $\sim$ 120 pc below the galactic plane), which is thought to be associated with the molecular cloud complex of G192-67 (Grant 1999), is also located in this clumpy LB wall region.

In the direction of the galactic center, lying very close to the galactic plane, are two small holes in the distribution of dense neutral gas lying beyond the nominal LB boundary surrounding the two regions containing the stars 51 Oph (d = 131 pc) and μ^1 Sco & λ Sco (d = 215–250 pc). These regions of small NaI equivalent width can also be clearly identified in Fig. 3. Close inspection of our data shows that the LB boundary is currently being defined Fig. 4 by stars lying well above and below the meridian plane in this particular direction. It is clear that in the direction along (or close to) the meridian there exists a gap in the neutral LB boundary that extends at least as far as the star λ Sco at a distance of $\sim$ 250 pc.

4.4. The LISM in the rotation plane – Fig. 5

In this projection we are viewing the LB along the galactic plane at right angles to the galactic center direction. Combining this view perpendicularly with that of Fig. 4 gives a quasi 3-D view of the LB in directions towards both galactic poles. Owing to observational selection effects the projectional view of the LB shown in Fig. 5 contains significantly fewer target stars than the previous two projections. However, the LB cavity is seen to posses a slightly enhanced radial bulge in the galactic plane and tapers towards the south galactic pole. Several of the features already mentioned in the two previously discussed projections can be readily identified in Fig. 5. For example, we note the δ Cyg gas cloud at a distance of $\sim$ 50 pc and the gas surrounding 2 Cet at a distance of $\sim$ 70 pc both residing within the LB cavity.

We also note the small 50 mÅ contour extension of the LB cavity dipping below the galactic plane to a distance of $\sim$ 150 pc in the direction of $l \sim 90°$ $b \sim$ -33°. This region, which contains stars associated with the molecular cloud complexes of MBM 53, MBM 54 and MBM 55 has been observed in NaI by Welty et al. (1989). Our data suggests that the nearest of these molecular cloud complexes is MBM 55 (defined by the level of absorption observed towards the star HD 217339) located at a distance of 100 pc at the very edge of the LB wall.

Although we do not have many data points for lines-of-sight with distances $>$ 150 pc for high galactic latitudes, Figs. 4 and 5 both suggest that the LB probably extends well into the halo, and thus is likely to be "open-ended". Several theories concerning supernovae events predict that hot, ionized gas can escape from the galactic plane and into the halo via the galactic fountain effect through interstellar chimneys (Edgar & Chevalier 1986). Our data indicate that leakage of hot, ionized gas into the halo from a possible past LB supernova event could well have occurred and a neutral gas boundary at high galactic latitudes has yet to fully form around the LB cavity. Clearly more, distant targets at high galactic latitude are required to determine whether the LB is completely open-ended or infact has a clumpy boundary interspersed with low column density lines-of-sight (i.e. like a kitchen colander). Supporting evidence for an open-ended LB is found in the detection of at least 13 extragalactic sources by the Extreme Ultraviolet Explorer satellite, all of which have sight-lines with high galactic latitudes ($b > 50°$) and modest neutral hydrogen column densities of N(HI) $\sim 10^{20}$ cm^{-2} (Marshall et al. 1995). Additionally we note that our current maps are also consistent with the low value of N(HI) observed towards the extragalactic sight-line of the Lockman Hole at l = 147° $b = 54°$.

4.5. Comparison with soft X-ray background maps

Snowden et al. (1998) have used the ROSAT soft X-ray all-sky survey maps to demonstrate that emission from the LB hot plasma dominates the 1/4 keV background at low galactic latitudes (as well as contributing much to the observed background flux at high latitudes). The intensity of the emission from an assumed 1 million degree K hot plasma was used to estimate the radial extent of the LB from the Sun, noting that variations in the observed soft X-ray emission were strongly anticorrelated with the total line-of-sight neutral HI column density. Since an optical depth of unity is obtained with a hydrogen column density of $\sim 10^{20}$ cm^{-2} for 1/4 keV X-rays, then if the LB is filled entirely with hot gas there should be a close correspondance between the distance distribution of soft X-ray background emission and our maps of the neutral NaI absorption 20–50mÅ boundary to the LB.

In Fig. 6(a)to(c) we show plots of the LB radius derived from our NaI absorption data in each of the 3 galactic projections and compare these to the equivalent LB contours derived by Snowden et al. (1998) from the ROSAT soft X-ray data (binned at an angular scale of 10 °). The first observation from these plots is that the LB contours derived from our NaI neutral gas absorption data occupy a far larger volume than those derived from the soft X-ray data. Although there is little detailed similarity between any of these three maps, there is a general concordance such that for all three projections the radius of both the NaI and soft X-ray derived LB contours is $>$ 50 pc.

In Fig. 6(a) we note that the third galactic quadrant (l = 180 - 270°) shows LB extensions well beyond 50 pc for both the NaI and soft X-ray data, with the NaI absorption map indicating a much larger extension of the LB to a distance of at least 200 pc. Also we note that an extension of the LB in the direction of Lupus-Norma (l = 330°) is present only in the NaI absorption contour and not in the soft X-ray data.

In order to reconcile the large-scale gross contours of the soft X-ray emitting LB with those inferred by the present NaI absorption data we note that the distance scale for soft X-ray background emission used by Snowden et al. was fixed using a distance to the MBM 12 cloud that resulted in a nominal LB radius of 40–130 pc. If a distance of 90 pc to the MBM cloud complex had been used (as discussed for the star ϵ Ari in Sect. 4.3)

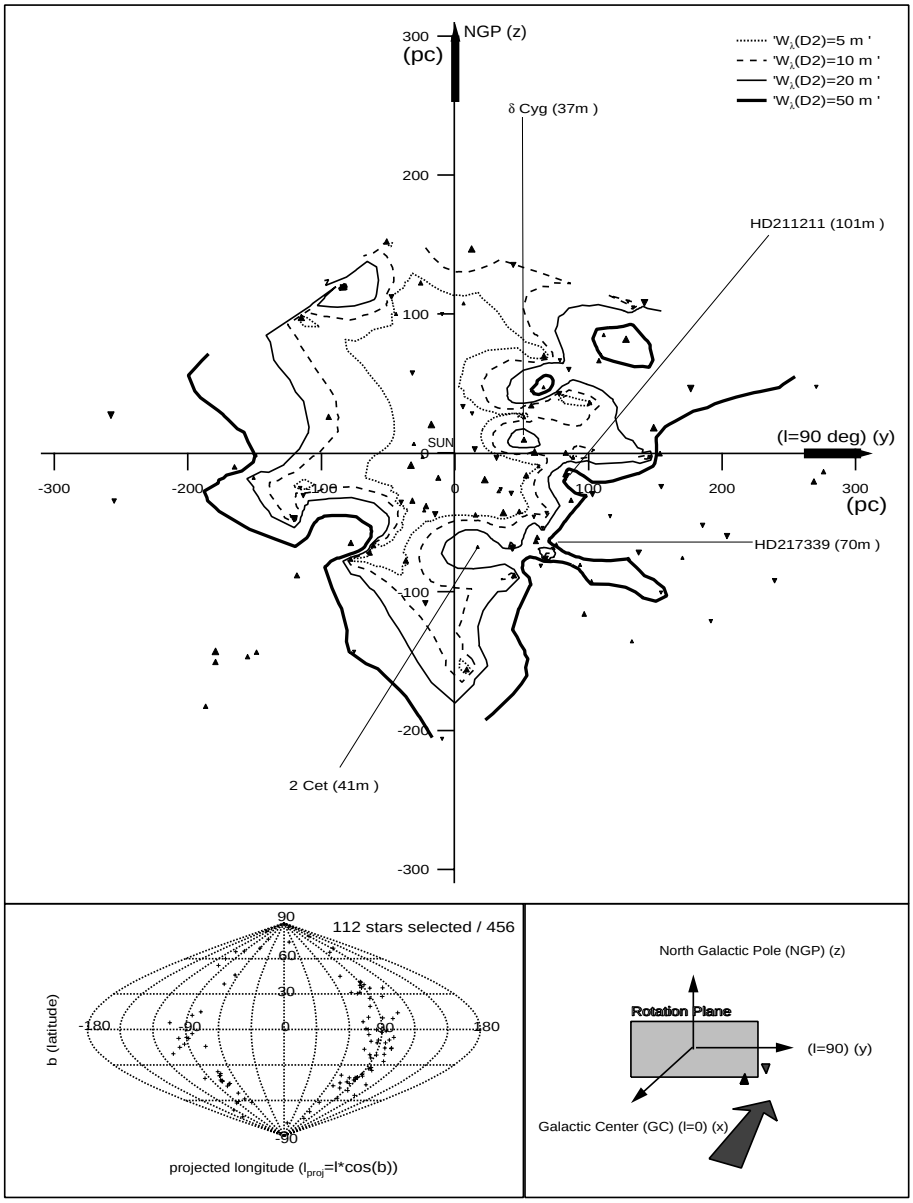

Fig. 5. Derived D2 absorption contours at 5, 10, 20 and 50 mÅ(m is for mÅ) for stars (represented on the plot as triangles) projected onto the Rotation Plane. We also show the galactic distribution of the 112 stars selected and a pictorial representation of the projection used.

this would have resulted in a range of soft X-ray emitting radii to the LB of 60–190 pc, far more consistent with our presently derived NaI absorption contours. This increase of 50 % in the absolute distance scale for the soft X-ray emission is consistent with the model of Snowden et al. for an inferred emission measure for the hot emitting plasma of 0.00223 cm^{-6} pc and an electron density of 0.005 cm^{-2}. However, this increase in LB size raises problems for the current soft X-ray model in that the derived pressure in the LB would be $\sim$ 30 % lower than the value of P/$k \sim$ 15,000 cm^{-3} K found previously by several authors (Berghofer et al. 1998, Burrows & Guo 1998). This may easily be accounted for since the ROSAT soft X-ray emission measures were derived from models that assumed both thermal ionization equilibrium and solar abundances, which may well not be appropriate for the LB hot gas (see Sect. 1).

5. Conclusion

We have carried out high spectral resolution (3 km s^{-1}) observations of the line-of-sight absorption of the NaI D1 and D2 interstellar lines towards 143 stars located within 300 pc of the Sun. From these data and previous measurements we have constructed maps of the galactic distribution of neutral sodium absorption towards a total of 456 stars in the local interstellar medium using three different galactic projections. Using these maps we have been able to better define the contours of the neutral absorption boundary (or "wall") to the Local Bubble cavity. Although this work represents the first phase of an extended program devoted to defining the contours of the LB and its kinematics, these preliminary maps clearly reveal the Local Bubble region as a low neutral density interstellar cavity with radii between 65–250 pc that is surrounded by a dense neutral

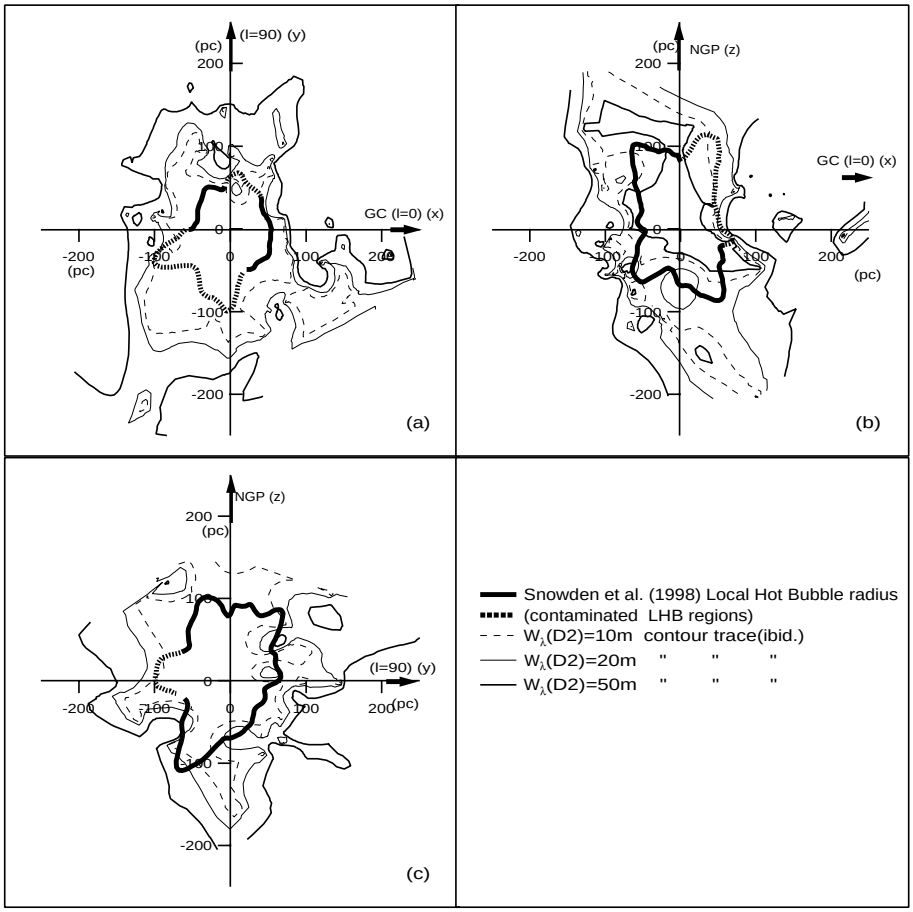

Fig. 6. Plots of the LB Na-D2 absorption contours in the three galactic projections of Figs. 3, 4 and 5 compared with contours of the Hot Local Bubble derived by Snowden et al. (1998) using ROSAT soft X-ray data. See legend for plotting details. m is for mÅ

gas wall. We have detected only one relatively dense accumulation of cold, neutral gas within 60 pc of the Sun that surrounds the star δ Cyg, and note that the nearest molecular cloud complexes of MBM 12 and MBM 53–55 are located at the edge of the neutral wall of the LB at a distance of ~ 90 pc. Our absorption maps also show that the LB extends at least as far as ~ 150 pc towards both galactic poles and is probably being "squeezed" in the galactic plane by the expansion of the surrounding shells of the Sco-Cen and Perseus-Taurus OB associations.

Work is in progress on observation of additional targets stars, especially at high latitudes. However, already we find it encouraging that some details and properties derived from these preliminary contours seem to make sense when compared with other independent measurements. As an example, the locations of the two stars ϵ and β CMa respectively inside and at the border of the LB may explain the strong differences between their observed line-of-sight aborbing gas quantities and properties. Additionally, the observed tilt of the LB cavity in the meridian plane is consistent with what one expects if the Gould Belt stellar associations are responsible for the squeezing of the Local Bubble.

We have compared our neutral gas contours of the LB with those derived by Snowden et al. 1998 using ROSAT soft X-ray background emission data. Although there is no detailed similarity between both maps, consistency between the global dimensions of both sets of contours is found for the case of a million degree hot plasma with an emission measure of $0.0023\,\mathrm{cm}^{-6}$ pc and an electron density of $0.005\,\mathrm{cm}^{-3}$. Such a model would infer a pressure in the LB of $\sim 10{,}000\,\mathrm{cm}^{-3}$ K, which is about 30% lower than that currently found by other authors.

Acknowledgements. We wish to thank the staff of the Observatoire de Haute Provence in France for their great help in performing these observations. We also thank Dr. Nahide Craig and Dr. John Vallerga for their assistance and advice. DS and BYW acknowledge funding support through Dr. Oswald Siegmund and the NASA FUSE program.

References

Benjamin R.A., Venn K.A., Hiltgen D.D., Sneden C., 1996, ApJ 464, 831
Berghoefer T., Bowyer S., Lieu R., Knude J., 1998, ApJ 500, 838
Bertin P., Lallement R., Ferlet R., Vidal-Madjar A., 1993, A&A 278, 549
Breitschwerdt D., Egger R., Freyberg M., Frisch P., Vallerga J., 1996, Space Sci. Rev. 78, 183
Burrows D.N., Guo Z., 1998, In: Breitschwerdt D., Freyberg M.J., Truemper J. (eds.) Lecture Notes in Physics Vol. 506, The Local Bubble and Beyond. Springer-Verlag, Berlin, p. 279
Cassinelli J., Cohen D., MacFarlane J., et al., 1995, ApJ 438, 932
Cassinelli J., Cohen D., MacFarlane J., al., 1996, ApJ 460, 949
Crawford I.A., 1991, A&A 247, 183
Crawford I.A., Craig N., Welsh B.Y., 1997, A&A 478, 648
Dupin O., Gry C., 1998, A&A 335, 661

Edgar R., Chevalier R., 1986, ApJ 310, L27
Egger R., Aschenbach B., 1995, A&A 294, L25
ESA, 1997, The Hipparcos Catalogue, ESA SP-1200
Ferlet R., Vida-Madjar A., Gry C., 1985, ApJ 298, 838
Genova R., Beckman J., Bowyer S., Spicer T., 1997, ApJ 484, 761
Grant C.E., Burrows N,D., 1999, ApJ submitted
Gry C., York D., Vidal-Madjar A., 1985, ApJ 296, 593
Gry C., Lemonon L., Vidal-Madjar A., Lemoine M., Ferlet R., 1995, A&A 302, 497
Heiles C., 1998, ApJ 498, 689
Hobbs L.M., 1978, ApJ 222, 491
Hobbs L.M., Blitz L., Magnani L., 1986, ApJ 306, L109
Hobbs L.M., Welty D., 1991, ApJ 368, 426
Izmodenov V.V., Lallement R., Malama Y.G., 1999, A&A 342, L13
Jelinsky P., Vallerga J., Edelstein J., 1995, ApJ 442, 653
Lallement R., Bertin P., Chassefiere E., Scott N., 1993, A&A 271, 734
Lallement R., Ferlet R., Lagrange A.M., Lemoine M., Vidal-Madjar A., 1995, A&A 304, 461
Lallement R., 1998, In: Breitschwerdt D., Freyberg M.J., Truemper J. (eds.) Lecture Notes in Physics Vol. 506, The Local Bubble and Beyond. Springer-Verlag, Berlin, p. 19
Lyons M.A., Bates B., Kemp S.N., 1994, A&A 286, 535
Lyu C.-H., Bruhweiler F., 1996, ApJ 459, 216
Marshall H., Fruscione A., Carone T., 1995, ApJ 439, 90
McKee C.F., Ostriker J.P., 1977, ApJ 218, 148
Mebold U. Kerp J., Kamberla P.M.W., 1998, In: Breitschwerdt D., Freyberg M.J., Truemper J. (eds.) Lecture Notes in Physics Vol. 506, The Local Bubble and Beyond. Springer-Verlag, Berlin, p. 199
Meyer D.M., Blades J.C., 1996 ApJ 464, L179
Moritz P., Wennmacher A., Herbstmeier U., Mebold U., Egger R., Snowden, S., 1998, A&A 336, 682
Park S., Finley J., Snowden S., Dame T., 1997, ApJ 476, 77
Penprase B., 1993, ApJS 88, 433
Penprase B.E., Lauer J., Aufrecht J., Welsh B.Y., 1998, ApJ 492, 617
Sahu M.S., Blades J.C., He L., et al., 1998, ApJ 504, 522
Sfeir D.M., 2000, Ph.D. Thesis, University of Paris VI (in preparation)
Slavin J., 1998, In: Breitschwerdt D., Freyberg M.J., Truemper J. (eds.) Lecture Notes in Physics Vol. 506, The Local Bubble and Beyond. Springer-Verlag, Berlin, p. 169
Snowden S., Cox D., McCammon D., Sanders W., 1990, ApJ 354, 211
Snowden S.L., Egger R., Finkbeiner D., Freyberg M., Plucinsky P., 1998, ApJ 493, 715
Welsh B.Y., 1991, ApJ 373, 556
Welsh B.Y., Craig N., Vedder P.W., Vallerga J.V., 1994, ApJ 437, 638
Welsh B.Y., Crifo F., Lallement R., 1998, A&A 333, 101 (Paper I)
Welsh B. Y., Sasseen T., Craig N., Jelinsky S., Albert C.E., 1997, ApJS 112, 507
Welty D.E., Hobbs. L.M., Blitz L., Penprase B., 1989, ApJ 346, 232
Welty D.E., Hobbs L.M., Kulkarni V., 1994, ApJ 436, 152
Welty D., Morton D., Hobbs L.M., 1996, ApJS 106, 533